Article

Aza Cope Rearrangement of Propargyl Enammonium Cations Catalyzed By a Self-Assembled "Nanozyme"

Courtney J. Hastings, Dorothea Fiedler, Robert G. Bergman, and Kenneth N. Raymond

J. Am. Chem. Soc., **2008**, 130 (33), 10977-10983 • DOI: 10.1021/ja8013055 • Publication Date (Web): 25 July 2008

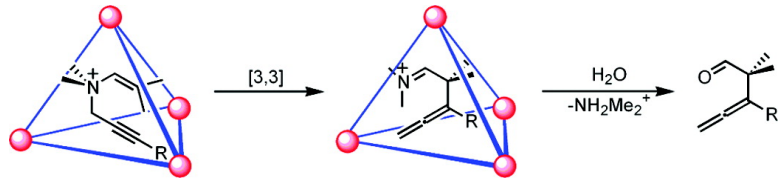

More About This Article

Additional resources and features associated with this article are available within the HTML version:

- Supporting Information
- Links to the 1 articles that cite this article, as of the time of this article download
- Access to high resolution figures
- Links to articles and content related to this article
- Copyright permission to reproduce figures and/or text from this article

View the Full Text HTML

J|A|C|S
ARTICLES

Published on Web 07/25/2008

Aza Cope Rearrangement of Propargyl Enammonium Cations Catalyzed By a Self-Assembled "Nanozyme"

Courtney J. Hastings, Dorothea Fiedler, Robert G. Bergman,* and Kenneth N. Raymond*

Department of Chemistry, University of California, Berkeley, California, 94720-1460

Received February 27, 2008; E-mail: rbergman@berkeley.edu; raymond@socrates.berkeley.edu

Abstract: The tetrahedral assembly $[Ga_4L_6]^{12-}$ [L = *N,N*-bis(2,3-dihydroxybenzoyl)-1,5-diaminonaphthalene) encapsulates a variety of cations, including propargyl enammonium cations capable of undergoing the aza Cope rearrangement. For propargyl enammonium substrates that are encapsulated in the $[Ga_4L_6]^{12-}$ assembly, rate accelerations by factors of up to 184 compared with the background reaction rate were observed. After rearrangement, the product iminium ion is released into solution and hydrolyzed, allowing for catalytic turnover. The activation parameters for the catalyzed and uncatalyzed reaction were determined, revealing that a decrease in the entropy of activation is responsible for the observed rate enhancements. The catalyzed reaction exhibits saturation kinetics: the rate data obeyed the Michaelis−Menten model of enzyme kinetics, and competitive inhibition using a nonreactive guest was demonstrated.

Introduction

In nature, enzymes utilize steric confinement and carefully positioned functional groups to catalyze reactions with high degrees of activity and selectivity.[1–4] The extraordinary efficiency of enzymes under mild physiological conditions has challenged chemists to design enzyme mimics with the goals of achieving useful catalytic processes and furthering our understanding of enzymes. To emulate this mode of catalysis, many research groups have designed synthetic hosts capable of binding and directing the reactivity of guest molecules.[5–13] Upon encapsulation in either a synthetic host or an enzyme active site, the environment surrounding a guest molecule differs drastically from that of the bulk solution. Steric constraints, positioning of functional groups, and sequestration from other molecules can enforce reactivity and selectivity that is impossible when simpler catalysts are employed.[8,13] Early work using crown ethers, cryptands, and cyclodextrins demonstrated the ability of molecular hosts to bind guests and influence chemical reactivity.[14–16] The development of host-mediated reactivity demands the creation of larger and more complex synthetic hosts, which in turn requires time-consuming multistep syntheses. As an alternative to covalent syntheses, chemists have designed large, well-defined structures that self-assemble from relatively simple subunits. Such supramolecular structures rely on weak, reversible interactions, such as hydrogen bonding or metal−ligand interactions, that are programmed into the subunits to form a single, thermodynamically stable assembly. This synthetic strategy provides access to complex structures in far fewer steps than those involved with traditional synthetic strategies and has thus become a popular method for preparing large host assemblies.[10,12,17,18]

Raymond and co-workers[19–22] have developed a series of self-assembled supramolecular metal−ligand assemblies having M_4L_6 stoichiometry [M = Ga^{3+} (**1**), Al^{3+}, Fe^{3+}; L = *N,N′*-bis(2,3-dihydroxybenzoyl)-1,5-diaminonaphthalene]. The four trivalent metal atoms are located at the vertices of a tetrahedron, and the naphthalene-based bis-bidentate catechol ligands span its edges, forming a *T*-symmetric, cavity-containing assembly (Figure 1). Strong mechanical coupling between the metal vertices through the ligands enforces self-assembly of a racemic

(1) Jencks, W. P. *Catalysis in Chemistry and Enzymology*; McGraw-Hill: New York, 1969.
(2) Kirby, A. J. *Angew. Chem., Int. Ed. Engl.* **1996**, *35*, 707–724.
(3) Tramontano, A.; Janda, K. D.; Lerner, R. A. *Science* **1986**, *234*, 1566–1570.
(4) Borman, S. *Chem. Eng. News* **2004**, *82*, 35–39.
(5) Hof, F.; Craig, S. L.; Nuckolls, C.; Rebek, J. *Angew. Chem., Int. Ed.* **2002**, *41*, 1488–1508.
(6) Kleij, A. W.; Reek, J. N. H. *Chem.—Eur. J.* **2006**, *12*, 4218–4227.
(7) Koblenz, T. S.; Wassenaar, J.; Reek, J. N. H. *Chem. Soc. Rev.* **2008**, *37*, 247–262.
(8) Lützen, A. *Angew. Chem., Int. Ed.* **2005**, *44*, 1000–1002.
(9) Motherwell, W. B.; Bingham, M. J.; Six, Y. *Tetrahedron* **2001**, *57*, 4663–4686.
(10) Oshovsky, G. V.; Reinhoudt, D. N.; Verboom, W. *Angew. Chem., Int. Ed.* **2007**, *46*, 2366–2393.
(11) Sanders, J. K. M. *Chem.—Eur. J.* **1998**, *4*, 1378–1383.
(12) Schmuck, C. *Angew. Chem., Int. Ed.* **2007**, *46*, 5830–5833.
(13) Vriezema, D. M.; Aragonès, M. C.; Elemans, J. A. A. W.; Cornelissen, J. J. L. M.; Rowan, A. E.; Nolte, R. J. M. *Chem. Rev.* **2005**, *105*, 1445–1489.
(14) Breslow, R.; Dong, S. D. *Chem. Rev.* **1998**, *98*, 1997–2012.
(15) Cram, D. J. *Angew. Chem., Int. Ed. Engl.* **1988**, *27*, 1009–1020.
(16) Lehn, J.-M. *Angew. Chem., Int. Ed. Engl.* **1988**, *27*, 89–112.
(17) Yeh, R. M.; Davis, A. V.; Raymond, K. N. Supramolecular Systems: Self-Assembly. In *Comprehensive Coordination Chemistry II*; McCleverty, J. A., Meyer, T. J. Eds. Elsevier: Oxford, U.K., 2004; pp 327−355.
(18) Mimassi, L.; Guyard-Duhayon, C.; Rager, M. N.; Amouri, H. *Inorg. Chem.* **2004**, *43*, 6644–6649.
(19) Caulder, D. L.; Bruckner, C.; Powers, R. E.; Konig, S.; Parac, T. N.; Leary, J. A.; Raymond, K. N. *J. Am. Chem. Soc.* **2001**, *123*, 8923–8938.
(20) Caulder, D. L.; Powers, R. E.; Parac, T. N.; Raymond, K. N. *Angew. Chem., Int. Ed.* **1998**, *37*, 1840–1843.
(21) Caulder, D. L.; Raymond, K. N. *J. Chem. Soc., Dalton Trans.* **1999**, 1185–1200.
(22) Caulder, D. L.; Raymond, K. N. *Acc. Chem. Res.* **1999**, *32*, 975–982.

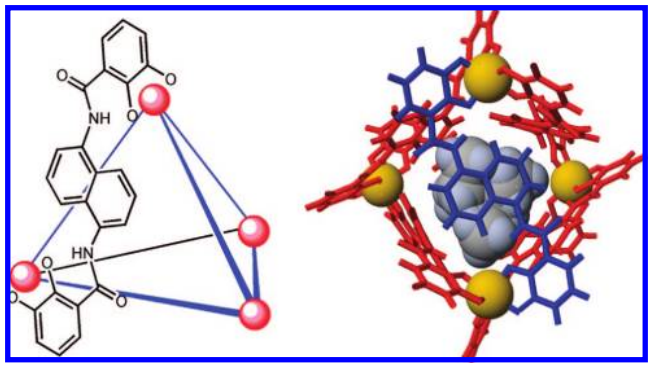

Figure 1. (left) Schematic of the $[Ga_4L_6]^{12-}$ assembly **1**; for clarity, only one ligand is shown. (right) Model of **1** with a tetraethylammonium cation guest, viewed down the twofold axis.

mixture of the homochiral ΔΔΔΔ and ΛΛΛΛ configurations. The two enantiomers can be resolved and are configurationally stable.[23,24]

A variety of monocationic guests, ranging from simple alkylammonium cations to transition-metal sandwich complexes, as well as neutral hydrophobic species such as alkanes can be encapsulated inside of **1**.[25] Molecules that are highly solvated in water, such as small monocations, are generally not encapsulated, while anionic molecules suffer from repulsive electrostatic interactions with the host that prevent their encapsulation. The overall charge of 12− on **1** imparts water solubility, while the naphthalene rings of the ligands enclose the interior cavity, providing a hydrophobic environment for guest molecules. These properties allow water-labile cations such as ketone-derived iminium ions,[26] diazonium and tropylium ions,[27] and reactive phosphine−acetone adducts[27,28] to be stabilized by encapsulation. While these cations are unstable and have very short lifetimes in aqueous solution, the polyanionic charge and hydrophobic cavity stabilize them.

The properties of **1** summarized above have been exploited to develop reactions that occur inside the cavity of **1** with higher degrees of reactivity and/or selectivity than when the reaction is performed in bulk solution. For example, the acid-catalyzed hydrolysis of acetals and orthoformates is catalyzed by **1** in basic solution.[29] Several encapsulated transition-metal complexes can participate in stoichiometric and catalytic organometallic reactions in which **1** imposes strict limits on the size and shape of substrates that will react.[30–32]

Pericyclic reactions are popular targets in supramolecular catalysis because encapsulation can by itself enforce the geometries necessary for enhanced reactivity, even in the absence of accelerating functional groups within the cavity. Diels−Alder reactions, for example, are particularly well-suited for this mode of catalysis, since binding of the diene and the dienophile into a constrictive environment dramatically increases the local concentration of these reactants. Rebek and co-workers[33–35] reported the first example of a host-mediated Diels−Alder reaction, and several reports from the Fujita research group have utilized a metal−ligand host to accelerate the Diels−Alder reaction of unreactive dienes.[36,37] In both systems, product inhibition was observed unless the affinity of the Diels−Alder adduct for the host interior was weaker than that of the reactants.[34,37] Thus, low levels of discrimination between the reactants and products of host-accelerated reactions are a major limitation of these reactions.

One strategy that can be used to circumvent this problem is the continuous conversion of the product into a species that is bound weakly by the host. We employed this approach in the catalysis of the sigmatropic rearrangement of allyl enammonium cations using metal−ligand assembly **1** and performed a detailed study of the mechanism of this reaction.[38,39] The 3-aza Cope rearrangement first converts an allyl enammonium cation to a γ,δ-unsaturated iminium cation via [3,3]-sigmatropic rearrangement, after which the iminium cation is hydrolyzed to the corresponding aldehyde.[40,41] This reaction is catalyzed by **1**, and rate enhancements by factors of up to 854 were measured.[38] Although the product iminium ion is encapsulated in **1**, hydrolysis converts this species to a neutral aldehyde that is much more weakly encapsulated, thereby allowing for catalytic turnover. The activation parameters for both the free and assembly-mediated reactions were determined for several substrates, and while the enthalpies of activation ($\Delta H^{\ddagger}$) for the free and assembly-mediated cases were nearly identical, the entropies of activation ($\Delta S^{\ddagger}$) for reactions of encapsulated guests were less negative than those for the reactions in free solution. This strongly suggested that a major component of the observed rate enhancement was the preorganization of the encapsulated substrate into a chairlike conformation that closely resembles the transition state of the sigmatropic rearrangement. This hypothesis was confirmed by a NOESY experiment that showed strong correlations between the two ends of the linear enammonium cation.[38]

Having investigated the catalysis of the aza Cope rearrangement of allyl enammonium ions using **1**, we were interested in extending the scope of this reaction to include propargyl enammonium substrates (Scheme 1). These compounds react at a much slower rate than the allyl−vinyl substrates, necessitating elevated temperatures to obtain useful rates of reaction. For this reason, we sought to determine whether encapsulation within **1** would accelerate this more challenging reaction. Furthermore, having observed in our original studies that rate

(23) Terpin, A. J.; Ziegler, M.; Johnson, D. W.; Raymond, K. N. *Angew. Chem., Int. Ed.* **2001**, *40*, 157–160.
(24) Ziegler, M.; Davis, A. V.; Johnson, D. W.; Raymond, K. N. *Angew. Chem., Int. Ed.* **2003**, *42*, 665–668.
(25) Biros, S. M.; Bergman, R. G.; Raymond, K. N. *J. Am. Chem. Soc.* **2007**, *129*, 12094–12095.
(26) Dong, V. M.; Fiedler, D.; Carl, B.; Bergman, R. G.; Raymond, K. N. *J. Am. Chem. Soc.* **2006**, *128*, 14464–14465.
(27) Fiedler, D.; Pagliero, D.; Brumaghim, J. L.; Bergman, R. G.; Raymond, K. N. *Inorg. Chem.* **2004**, *43*, 846–848.
(28) Ziegler, M.; Brumaghim, J. L.; Raymond, K. N. *Angew. Chem., Int. Ed.* **2000**, *39*, 4119–4121.
(29) Pluth, M. D.; Bergman, R. G.; Raymond, K. N. *Science* **2007**, *316*, 85.
(30) Leung, D. H.; Bergman, R. G.; Raymond, K. N. *J. Am. Chem. Soc.* **2006**, *128*, 9781–9797.
(31) Leung, D. H.; Bergman, R. G.; Raymond, K. N. *J. Am. Chem. Soc.* **2007**, *129*, 2746–2747.
(32) Leung, D. H.; Fiedler, D.; Bergman, R. G.; Raymond, K. N. *Angew. Chem., Int. Ed.* **2004**, *43*, 963–966.
(33) Kang, J. M.; Hilmersson, G.; Santamaria, J.; Rebek, J. *J. Am. Chem. Soc.* **1998**, *120*, 3650–3656.
(34) Kang, J. M.; Rebek, J. *Nature* **1997**, *385*, 50–52.
(35) Kang, J. M.; Santamaria, J.; Hilmersson, G.; Rebek, J. *J. Am. Chem. Soc.* **1998**, *120*, 7389–7390.
(36) Nishioka, Y.; Yamaguchi, T.; Yoshizawa, M.; Fujita, M. *J. Am. Chem. Soc.* **2007**, *129*, 7000–7001.
(37) Yoshizawa, M.; Tamaru, M.; Fujita, M. *Science* **2006**, *312*, 251–254.
(38) Fiedler, D.; Bergman, R. G.; Raymond, K. N. *Angew. Chem., Int. Ed.* **2004**, *43*, 6748–6751.
(39) Fiedler, D.; van Halbeek, H.; Bergman, R. G.; Raymond, K. N. *J. Am. Chem. Soc.* **2006**, *128*, 10240–10252.
(40) Elkik, E.; Francesch, C. *Bull. Soc. Chim. Fr.* **1968**, *3*, 903–910.
(41) Opitz, G. *Justus Liebigs Ann. Chem.* **1961**, 122–132.

Scheme 1. General Reaction Scheme for the 3-Aza Cope Rearrangement[a]

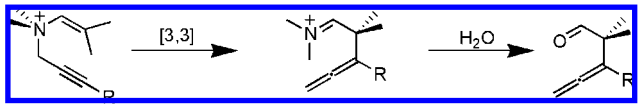

[a] Starting from a propargyl enammonium cation, [3,3]-sigmatropic rearrangement leads to an allenyl iminium cation, which then hydrolyzes to an allenyl aldehyde.

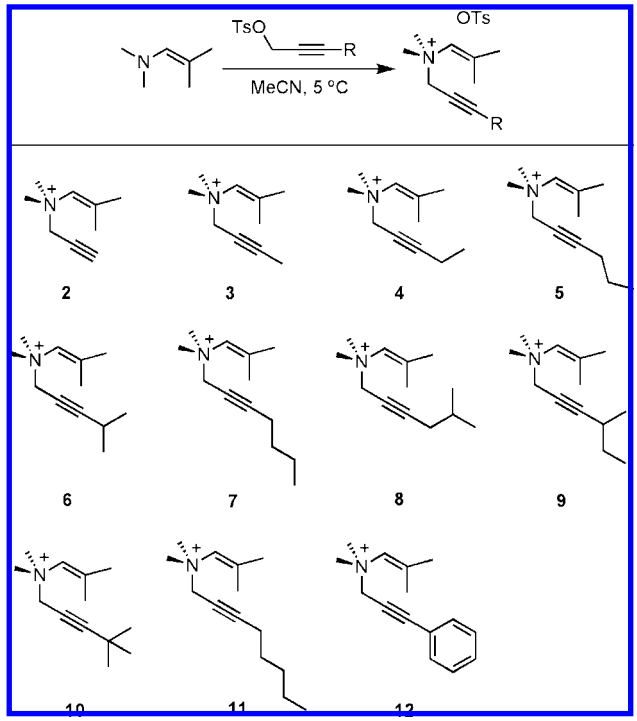

Figure 2. Synthesis of the propargyl enammonium substrates.

enhancements are highly shape-selective, we were interested in studying the propargyl compounds, which cannot adopt the same conformations as the vinyl substrates. Here we present the extension of our previous work to include the propargyl enammonium substrate class.

Results and Discussion

Encapsulation and Rate Acceleration. A series of propargyl enammonium tosylates with various alkyl substituents at the alkyne terminus was prepared (Figure 2). These substrates were synthesized by alkylation of *N,N*-dimethylisobutenylamine with the corresponding propargyl tosylate in yields ranging from 15 to 89%. Crude yields were generally 80−90%, and the low yields reported for substrates **5**, **6**, **7**, and **10** were a result of inefficient recrystallizations necessary to obtain analytically pure material. Upon encapsulation in **1**, the guest resonances were shifted upfield 2−4 ppm as a result of the anisotropic ring current in the nearby naphthalene walls of **1**. Furthermore, encapsulation into the chiral interior of **1** renders enantiotopic guest protons diastereotopic. This typically affected the protons of the methylene group and the two *N*-methyl groups present in each substrate molecule. Host−guest complexes of compounds **2**−**9** were formed quantitatively in D_2O and DMSO-d_6, as determined by ^{1}H NMR. Additional evidence for these host−guest complexes was obtained by high-resolution electrospray mass spectrometry. Encapsulation occurred within minutes, and substrates could be ejected from the host interior by the addition of tetraethylammonium bromide, a strongly binding guest. Guests bearing more sterically demanding *tert*-butyl (**10**), *n*-pentyl (**11**), and phenyl (**12**) substituents were not encapsulated, demonstrating that encapsulation of these substrates is strongly size-dependent. It is noteworthy that among the four isomers bearing a butyl group at the alkyne terminus (**7**−**10**), only the *tert*-butyl-substituted substrate **10** was excluded from the host interior. These results suggest that butyl-substituted compounds are only encapsulated if they possess a certain degree of conformational flexibility, reflecting the shape-selectivity of **1**.

Table 1. Rate Constants for Background (k_{free}) and Encapsulated (k_{encaps}) Aza Cope Rearrangements of Various Substrates (Measured at 60 °C in D_2O) and the Corresponding Rate Accelerations

compound	R	k_{free} (10^{-8} s^{-1})	k_{encaps} (10^{-8} s^{-1})	k_{encaps}/k_{free}
2	H	62.4	237	4
3	Me	62.3	6200	100
4	Et	20.0	3670	184
5	*n*-Pr	19.5	1920	98
6	*i*-Pr	6.7	870	129
7	*n*-Bu	15.1	73	5
8	*i*-Bu	17.0	477	28
9	*s*-Bu	50.0	1150	23

After the scope of encapsulation was demonstrated, the rates of the aza Cope rearrangement and subsequent hydrolysis were measured for both free and encapsulated substrates. Reactions were monitored by ^{1}H NMR, and the reaction rates were based on the disappearance of starting material because of the insolubility of the product aldehydes in D_2O (product formation was observed by ^{1}H NMR when wet DMSO-d_6 was used as the solvent). The reaction rates of encapsulated enammonium cations were measured using a stoichiometric amount of **1**, and the background reaction was monitored in the absence of **1**. Clean first-order disappearance of starting material was observed in both the encapsulated and unencapsulated reactions, and the observed rate constants are shown in Table 1. For each substrate that was encapsulated by **1**(compounds **2**−**9**), encapsulation accelerated the rate of reaction by as much as 2 orders of magnitude compared with the free reaction. In the unencapsulated reaction, the substrates with larger groups at the alkyne terminus (**4**−**8**) reacted more slowly as a consequence of steric repulsion that disfavors the reactive chairlike conformation required in the transition state. However, in the reaction of encapsulated substrates, the fastest rates were observed for the medium-sized substrates (**3**−**6**), while the largest and smallest compounds reacted more slowly. This "optimal fit" trend was also observed in our earlier work on allyl enammonium guests.

Catalytic Kinetics. With the exception of **6**, the iminium rearrangement product was rapidly hydrolyzed to the corresponding aldehyde, leaving empty **1** behind. Previous studies have shown that the iminium hydrolysis step occurs outside the host cavity.[39] Encouraged by the regeneration of empty **1**, we explored the use of **1** as a catalyst for this reaction. Because of the relatively low rates of the reactions catalyzed by **1**, substrate **3**, which had the highest encapsulated reaction rate (i.e., the largest value of the rate constant k_{encaps}), was used to study the kinetics of the catalytic system. Kinetic analysis of the catalytic reaction of substrate **3** showed that when more than 3 equiv of substrate is present, the overall reaction is zeroth order in substrate (Figure 3). This suggests that the encapsulated starting material is the resting state of the catalyst and that the rate-limiting step of the reaction is the sigmatropic rearrangement

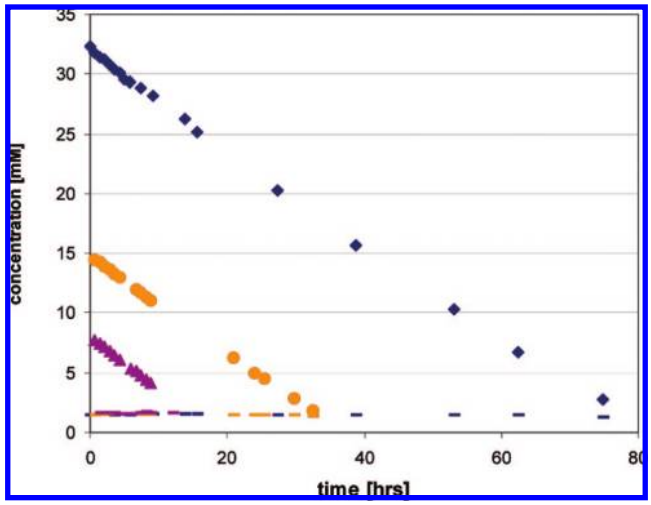

Figure 3. Plots of concentration of unbound substrate **3** as a function of time for the catalytic aza Cope rearrangement of **3**. Initial concentrations of unbound starting material: blue triangles, 19 equiv of **3** with respect to **1**; orange circles, 9 equiv of **3**; purple triangles, 4.5 equiv of **3**. The concentration of host-bound substrate [**3** ⊂ **1**] corresponding to each unbound substrate concentration is indicated by the hyphen of the same color at the corresponding time.

of the bound substrate, which is followed by rapid product release and binding of an additional substrate molecule (Figure 4). Thus, the rate of reaction is dependent on the concentration of host-bound substrate rather than on the total concentration of substrate, leading to the following rate law: rate $= k_2$[**3** ⊂ **1**] (where ⊂ denotes encapsulation). Consistent with this rate law, under zeroth-order conditions, the observed concentration of [**3** ⊂ **1**] was invariant (Figure 3), confirming that the host-bound starting material [**3** ⊂ **1**] is the catalyst resting state. From the experimentally determined concentration of [**3** ⊂ **1**] and the observed rate of reaction, it was possible to determine the first-order rate constant k_2 that appears in the rate law. The value of k_2 so obtained was identical to the rate constant value determined from the first-order plot for the stoichiometric reaction of [**3** ⊂ **1**]. Thus, the proposed rate law describes both the stoichiometric and catalytic reactions. Throughout these experiments, the only encapsulated species present was the host-bound starting material [**3** ⊂ **1**]; encapsulation of the iminium rearrangement product was never observed. On the basis of these results together with the kinetic profile of this reaction, we can conclude that **1** is a true catalyst in the reaction and does not suffer from product inhibition.

Michaelis−Menten Analysis. In enzymatic catalysis, a substrate and enzyme typically participate in a reversible equilibrium with an enzyme−substrate complex, and the conversion of enzyme-bound substrate into enzyme-bound product is rate-determining. A consequence of this scenario is the observation of rate saturation at high substrate concentrations. The Michaelis−Menten kinetic model is most frequently used to understand this type of enzymatic pathway.[42] The Michaelis−Menten kinetic parameters of the catalyzed rearrangement ($V_{max} = 1.2 \times 10^{-4}$ mM s^{-1}, $K_m = 0.67$ mM, and $k_{cat} = 7.0 \times 10^{-5}$ s^{-1}, where V_{max} is the maximum velocity of the reaction, K_m is the Michaelis constant, and k_{cat} is the turnover rate of the bound substrate) were determined from an Eadie−Hofstee plot of the substrate saturation curve of **3**.[43,44] The calculated value V_{max} was identical to the maximum measured velocity of the reaction under saturation conditions, and the calculated value of k_{cat} was equal to the experimentally determined rate constant. In systems such as this, where a fast pre-equilibrium is established prior to the catalytic step (i.e., where k_1 and k_{-1} are much larger than k_2), the Michaelis constant K_m is essentially a dissociation constant (K_d). The value of K_m for **3** was larger than the K_d value for NEt_4^+ (5.1×10^{-2} mM) but smaller than that for NMe_4^+ (9.0 mM), which is consistent with the results of competitive binding experiments, where **3** displaced NMe_4^+ from [NMe_4^+ ⊂ **1**] and NEt_4^+ displaced **3** from [**3** ⊂ **1**].

A characteristic aspect of enzymatic catalysis is the inhibition of the enzyme active site with a suitable nonreactive molecule whose binding is competitive with that of the substrate.[42] A bound inhibitor excludes substrate from the active site, thereby inhibiting the activity of the enzyme. If binding of the substrate and the inhibitor is truly competitive, the inhibitor can be completely displaced if the substrate concentration is sufficiently high; thus, at infinite substrate concentration, the value of V_{max} will be equal to that of the uninhibited reaction. To perform these experiments using **1**, several nonreactive alkylammonium guests were considered as competitive inhibitors. In previous work, we determined that ionic strength has no effect on the rate of reaction, so we were not concerned about any salt effects from added alkylammonium species.[39] The resonances of encapsulated NMe_4^+ overlap with those of encapsulated **3**, and the displacement of strongly bound NEt_4^+ requires a large excess of **3**. Thus, neither NMe_4^+ nor NEt_4^+ was a suitable inhibitor for these experiments. However, the ^{1}H NMR resonances of encapsulated NPr_4^+ are easily resolved from those of encapsulated **3** (Figure 5), and the binding constants of these two species are on the same order of magnitude; thus, NPr_4^+ was an ideal inhibitor for these experiments.

Rate data under saturation conditions were collected in the presence of 4 or 10 equiv of NPr_4^+ with respect to **1**. Eadie−Hofstee plots of these data and of the saturation data obtained in the absence of inhibitor (Figure 6) were used to determine the corresponding Michaelis−Menten parameters.[43,44] As expected, a larger excess of substrate was required to reach the maximum reaction velocity in the presence of inhibitor, but the same V_{max} was eventually achieved. These experiments clearly demonstrate that NPr_4^+ acts as a competitive inhibitor in this system and that the kinetic behavior of this system is comparable to that found in our earlier studies of assembly-catalyzed orthoformate and acetal hydrolysis[29] as well as to the mode of action of enzymes.

Activation Parameters of the Catalytic Reaction. Our previous studies of the **1**-catalyzed aza Cope rearrangement revealed that decreases in $\Delta S^{\ddagger}$ were responsible for rate enhancements with respect to the background reaction. We sought to confirm that rate accelerations for rearrangement of the propargyl enammonium substrates studied here originate from the same entropic considerations. In addition, we wished to compare the changes in $\Delta S^{\ddagger}$ values for the present system to the previously reported values.

The variable-temperature kinetics of the catalyzed and uncatalyzed reactions of **3** were measured, and Eyring analyses of the resulting data provided activation parameters for the two reactions. For the uncatalyzed rearrangement of **3**, $\Delta H^{\ddagger} = 23$

(42) McKee, T.; McKee, J. R. *Biochemistry: The Molecular Basis of Life*, 3rd ed.; McGraw-Hill: New York, 2003.
(43) Eadie, G. S. *J. Biol. Chem.* **1942**, *146*, 85–93.
(44) Hofstee, B. H. J. *Science* **1952**, *116*, 329–331.

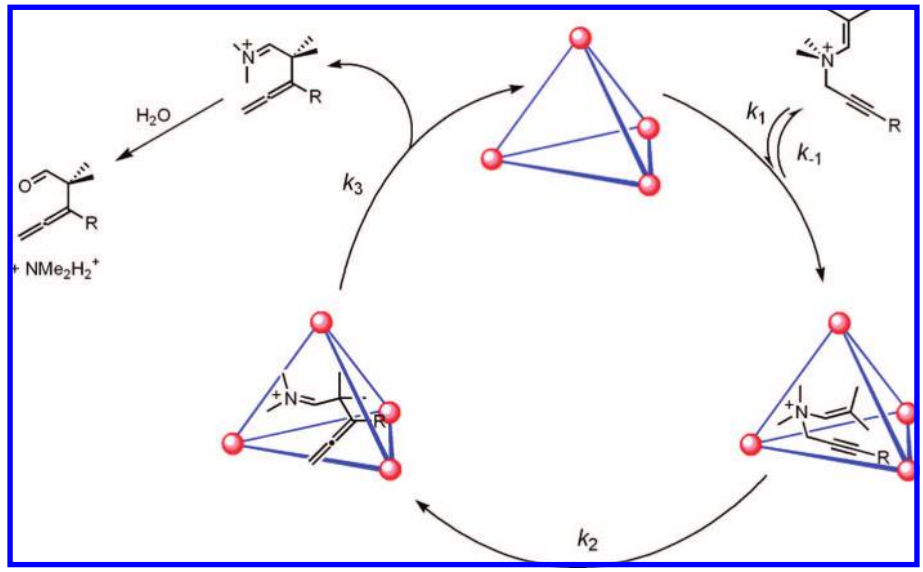

Figure 4. Proposed catalytic cycle for the propargyl 3-aza Cope rearrangement. The rearrangement of the encapsulated substrate (with rate constant k_2) is the rate-determining step.

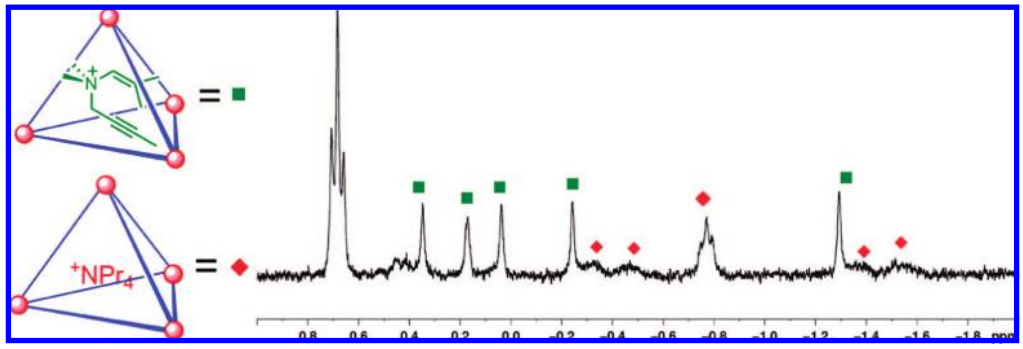

Figure 5. ^{1}H NMR spectrum of a sample containing 1 equiv each of **1**, substrate **3**, and NPr_4Br. Encapsulation is observed for both **3** and NPr_4^+.

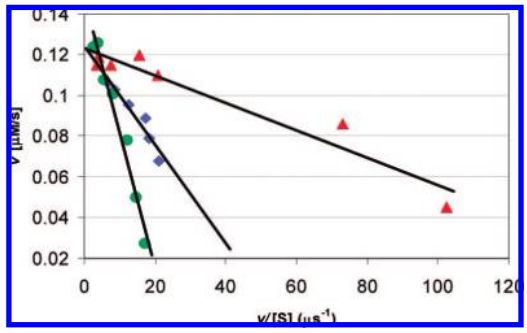

Figure 6. Eadie−Hofstee plots of inhibition data for the 3-aza Cope rearrangement of **3** catalyzed by **1**, using NPr_4^+ inhibitor: red triangles, no inhibitor added; blue diamonds, 4 equiv of NPr_4^+; green circles, 10 equiv of NPr_4^+.

$\pm$ 3 kcal/mol and $\Delta S^{\ddagger} = -19 \pm 4$ eu. The large negative $\Delta S^{\ddagger}$ value is a common feature of [3,3]-sigmatropic rearrangements, and it reflects the organized transition state that the molecule must adopt in this reaction. The $\Delta S^{\ddagger}$ value for this reaction is more negative than that measured for analogous allyl enammonium species, which accounts for the lower reactivity of the propargyl systems in the aza Cope rearrangement.[38] In general, however, $\Delta S^{\ddagger}$ for the [3,3]-sigmatropic rearrangment of 1,5-enynes is less negative than that of the corresponding 1,5 dienes, and no clear trend relating the activation parameters of these two classes of compounds has been identified.[45]

For the catalyzed rearrangement of **3**, $\Delta H^{\ddagger} = 26 \pm 5$ kcal/mol and $\Delta S^{\ddagger} = +2.8 \pm 0.9$ eu. This $\Delta S^{\ddagger}$ value is more positive than that of the background rearrangement by >20 eu, a dramatic change that strongly suggests that **1** selectively binds a preorganized, reactive conformation of the substrate. The bound substrate has fewer degrees of freedom in the confines of the assembly and cannot adopt the conformation that would be lowest in energy for the unencapsulated molecule. The difference in the enthalpy of activation between the two reactions is within the experimental error, so it is clear that the entropic component of this reaction determines the observed rate enhancements.

Conclusion

In summary, we have demonstrated that a supramolecular metal−ligand assembly catalyzes the aza Cope rearrangement of propargyl enammonium cations. While classical catalysis of such sigmatropic rearrangements typically requires a Lewis or Brønsted acid, substrate encapsulation within the confined host interior enforces a reactive conformation that accelerates the rate of rearrangement by factors of up to 184. Consistent with this explanation, the determination of the activation parameters

(45) Viola, A.; MacMillan, J. H. *J. Am. Chem. Soc.* **1970**, *92*, 2404–2410.

for the uncatalyzed and host-catalyzed reactions revealed that rate enhancements are due to a more positive value of $\Delta S^{\ddagger}$ for the catalytic rearrangement. The catalytic reaction obeys the Michaelis−Menten model of enzyme kinetics, and competitive inhibition of this reaction was observed using NPr_4^+, a nonreactive guest. These studies demonstrate how supramolecular hosts are able to act as enzyme mimics in the catalysis of challenging reactions under mild, aqueous conditions. While a large number of chemical reactions in nature are catalyzed by enzymes, synthetic chemists have only just begun to realize the potential of synthetic hosts in catalysis. As new supramolecular hosts are developed and their properties understood, we anticipate that many new examples of supramolecular catalysis will be discovered.

Experimental Section

General Considerations. Reactions and manipulations were performed using standard Schlenk and high-vacuum techniques at room temperature, unless otherwise noted. Glassware was dried in an oven at 150 °C overnight or flame-dried under vacuum prior to use. NMR spectra were obtained on Bruker Avance AV 300, AV 400, DRX 500, and AV-500 spectrometers. Chemical shifts (δ) are reported in parts per million (ppm) relative to residual protonated solvent resonances. In the case of D_2O samples, ^{13}C shifts were referenced to an internal standard of CD_3OD.[46] Coupling constants are reported in Hz. IR spectra were measured neat on a Nicolet Avatar 370 FT-IR spectrometer with a zinc selenide attenuated total reflective (ATR) accessory. Peak intensities are reported as broad (b), weak (w), medium (m), or strong (s). Only peaks in the functional group region (4000−1300 cm^{-1}) are reported.

Elemental analyses, low-resolution fast atom bombardment (FAB), high-resolution FAB, and high-resolution electrospray (ES) time-of-flight (TOF) mass spectrometry (MS) were performed at the University of California, Berkeley, Microanalytical Facility. Elemental analyses were performed on a PerkinElmer Series II CHNO/S analyzer. Reliable combustion analyses for the host−guest compounds were not possible because of varying amounts of solvent bound to the exterior of the assembly. FAB mass spectra were recorded on a Micromass ZAV2-EQ (magnetic sector) instrument. High-resolution TOF ES-MS of the host−guest complexes were recorded on a Waters QTOF API mass spectrometer equipped with a Z-spray source.

Unless otherwise noted, reagents were obtained from commercial suppliers and used without further purification. Anhydrous solvents were dried over activated alumina under nitrogen pressure and sparged with nitrogen before use.[47] *N,N*-Dimethylisobutenylamine,[48] 4-methyl-2-hexynol,[49] and 5-methyl-2-hexynol[50] were prepared according to published procedures.

General Procedure for Encapsulation Reactions. The potassium or sodium salt of **1** (3.0 mg, 0.85 μmol) and the enammonium tosylate (0.90 μmol) were combined in a vial and dissolved in 600 μL of D_2O. The solution was transferred to an NMR tube, and the spectrum was recorded within 20 min after dissolution. Samples for mass spectrometry were prepared in an identical fashion, using H_2O instead of D_2O. Samples were flushed with N_2 after mixing, and mass spectra were obtained within 12 h of sample preparation.

Analytical Data for Host−Guest Complexes Prepared As Described Above. In each of the following paragraphs, ◆ denotes the host−guest species for which the paragraph gives data.

K_{11}[2 ⊂ 1]. ^1H NMR (400 MHz, D_2O): δ 8.01 (d, ^3J = 7.6 Hz, 12H, Ar−*H*), 7.91 (d, ^3J = 6.8 Hz, 2H, OTs), 7.83 (d, ^3J = 8.4 Hz, 12H, Ar−*H*), 7.69 (d, ^3J = 8.4 Hz, 2H, OTs), 7.31 (d, ^3J = 8.4 Hz, 12H, Ar−*H*), 7.09 (t, ^3J = 8.4 Hz, 12H, Ar−*H*), 6.77 (d, ^3J = 7.2 Hz, 12H, Ar−*H*), 6.62 (d, ^3J = 8.0 Hz, 12H, Ar−*H*), 2.37 (s, 3H, OTs), 2.06 (s, 1H, C*H*, encaps.), 0.52 (s, 1H, C*H*, encaps.), 0.48 (s, 1H, C*H*, encaps.), 0.28 (d, ^4J = 16.0, 1H, C*H*, encaps.), −0.06 (s, 3H, CH_3, encaps.), −0.14 (s, 3H, CH_3, encaps.), −0.49 (s, 3H, CH_3, encaps.), −0.89 (s, 3H, CH_3, encaps.). TOF MS ES(−) *m*/*z* calcd (found): $Ga_4C_{153}H_{103}N_{13}O_{36}K_8$ [◆ − $3K^+$]$^{3-}$, 1096.0198 (1096.0209); $Ga_4C_{153}H_{105}N_{13}O_{36}K_6$ [◆ − $5K^+$]$^{4-}$, 802.53 (802.53).

K_{11}[3 ⊂ 1]. ^1H NMR (400 MHz, D_2O): δ 8.04 (s, br, 12H, Ar−*H*), 7.82 (d, ^3J = 7.6 Hz, 12H, Ar−*H*), 7.69, (d, ^3J = 8.0 Hz, 2H, OTs), 7.35 (d, ^3J = 8.4 Hz, 2H, OTs), 7.30 (d, ^3J = 7.6 Hz, 12H, Ar−*H*), 7.07 (t, ^3J = 7.6 Hz, 12H, Ar−*H*), 6.76 (d, ^3J = 6.8 Hz, 12H, Ar−*H*), 6.61 (t, ^3J = 7.6 Hz, 12H, Ar−*H*), 2.37 (s, 3H, OTs), 1.95 (s, 1H, C*H*, encaps.), 0.65 (s, 3H, CH_3, encaps.), 0.57 (d, 1H, C*H*, encaps.), 0.51 (d, 1H, C*H*, encaps.), 0.19 (s, 6H, CH_3, encaps.), −0.18 (s, 3H, CH_3, encaps.), −1.10 (s, 3H, CH_3, encaps.). TOF MS ES(−) *m*/*z* calcd (found): $Ga_4C_{154}H_{105}N_{13}O_{36}K_8$ [◆ − $3K^+$]$^{3-}$, 1100.692 (1100.693); $Ga_4C_{154}H_{106}N_{13}O_{36}K_7$ [◆ − $4K^+$]$^{4-}$, 815.776 (815.775).

K_{11}[4 ⊂ 1]. ^1H NMR (400 MHz, D_2O): δ 8.04 (d, ^3J = 7.6 Hz, 12H, Ar−*H*), 7.76 (d, ^3J = 8.8 Hz, 12H, Ar−*H*), 7.70 (d, ^3J = 7.7 Hz, 2H, OTs), 7.38 (d, ^3J = 8.0 Hz, 2H, OTs), 7.33 (d, ^3J = 8.0 Hz, 12H, Ar−*H*), 7.03 (t, ^3J = 8.0 Hz, 12H, Ar−*H*), 6.78 (d, ^3J = 6.8 Hz, 12H, Ar−*H*), 6.62 (t, ^3J = 8.0 Hz, 12H, Ar−*H*), 2.40 (s, 3H, OTs), 1.76 (s, 1H, C*H*, encaps.), 0.94 (d, ^2J = 15.7 Hz, 1H, C*H*, encaps.), 0.75 (s, 3H, CH_3, encaps.), 0.67 (s, 3H, CH_3, encaps.), 0.40 (s, 3H, CH_3, encaps.), 0.09 (d, ^2J = 15.4 Hz, 1H, C*H*, encaps.), −0.52 (m, 2H, CH_2, encaps.), −1.02 (s, 3H, CH_3, encaps.), −1.06 (t, ^3J = 7.6 Hz, 3H, CH_3, encaps.). TOF MS ES(−) *m*/*z* calcd (found): $Ga_4C_{155}H_{107}N_{13}O_{36}K_8$ [◆ − $3K^+$]$^{3-}$, 1105.364 (1105.364); $Ga_4C_{155}H_{108}N_{13}O_{36}K_7$ [◆ − $4K^+$]$^{4-}$, 819.280 (819.279).

K_{11}[5 ⊂ 1]. ^1H NMR (500 MHz, D_2O): δ 8.06 (d, ^3J = 7.5 Hz, 12H, Ar−*H*), 7.84 (d, ^3J = 9.0 Hz, 12H, Ar−*H*), 7.64 (d, ^3J = 7.5 Hz, 2H, OTs), 7.23 (d, ^3J = 7.5 Hz, 12H, Ar−*H*), 7.17 (d, ^3J = 7.5 Hz, 2H, OTs), 7.07 (t, ^3J = 8.0 Hz, 12H, Ar−*H*), 6.62 (d, ^3J = 6.5 Hz, 12H, Ar−*H*), 6.31 (t, ^3J = 7.5 Hz, 12H, Ar−*H*), 2.51 (s, 2H, CH_2, encaps.), 2.20 (s, 1H, C*H*, encaps.), 1.34 (s, 2H, CH_2, encaps.), 0.50 (q, ^3J = 12.8 Hz, 2H, CH_2, encaps.), 0.10 (s, 3H, CH_3, encaps.), 0.01 (s, 3H, CH_3, encaps.), −0.70 (s, 3H, CH_3, encaps.), −0.82 (s, 3H, CH_3, encaps.). TOF MS ES(−) *m*/*z* calcd (found): $Ga_4C_{156}H_{109}N_{13}O_{36}K_8$ [◆ − $3K^+$]$^{3-}$, 1110.035 (1110.044); $Ga_4C_{156}H_{110}N_{13}O_{36}K_7$ [◆ − $4K^+$]$^{4-}$, 822.784 (822.781).

K_{11}[6 ⊂ 1]. ^1H NMR (500 MHz, D_2O): δ 8.07 (d, ^3J = 6.5 Hz, 12H, Ar−*H*), 7.72−7.67 (m, 14H, Ar−*H* + OTs), 7.36 (d, ^3J = 8.0 Hz, 12H, Ar−*H*), 7.29 (d, ^3J = 8.0 Hz, 12H, Ar−*H*), 7.01 (t, ^3J = 8.0 Hz, 12H, Ar−*H*), 6.74 (d, ^3J = 7.0 Hz, 12H, Ar−*H*), 6.59 (t, ^3J = 8.0 Hz, 12H, Ar−*H*), 1.70 (s, 1H, C*H*, encaps.), 1.19 (d, 1H, C*H*, encaps.), 1.10 (s, 3H, CH_3, encaps.), 1.03 (s, 1H, C*H*, encaps.), 0.73 (s, 3H, CH_3, encaps.), −0.36 (d, 1H, C*H*, encaps.), −1.03 (s, 3H, CH_3, encaps.), −1.48 (s, 3H, CH_3, encaps.), −1.60 (s, 3H, CH_3, encaps.). TOF MS ES(−) *m*/*z* calcd (found): $Ga_4C_{156}H_{109}N_{13}O_{36}K_8$ [◆ − $3K^+$]$^{3-}$, 1110.036 (1110.009); $Ga_4C_{156}H_{110}N_{13}O_{36}K_7$ [◆ − $4K^+$]$^{4-}$, 822.784 (822.757).

Na_{11}[7 ⊂ 1]. ^1H NMR (500 MHz, D_2O): δ 8.06 (d, ^3J = 7.5 Hz, 12H, Ar−*H*), 7.75 (d, ^3J = 8.5 Hz, 12H, Ar−*H*), 7.70 (d, ^3J = 8.5 Hz, 2H, OTs), 7.36 (d, ^3J = 8.0 Hz, 2H, OTs), 7.33 (d, ^3J = 8.0 Hz, 12H, Ar−*H*), 6.99 (t, ^3J = 8.0 Hz, 12H, Ar−*H*), 6.79 (d, ^3J = 7.0 Hz, 12H, Ar−*H*), 6.62 (t, ^3J = 7.5 Hz, 12H, Ar−*H*), 2.01 (s, 1H, C*H*, encaps.), 1.49 (d, ^3J = 15 Hz, 1H, C*H*, encaps.), 1.24 (s, 3H, CH_3, encaps.), 0.66 (d, ^3J = 35.0 Hz, 6H, $(CH_3)_2$, encaps.), −0.05 (d, ^3J = 15.5 Hz, 1H, C*H*, encaps.), −0.206 (s, 2H, CH_2, encaps.), −0.958 (s, 3H, CH_3, encaps.), −1.042 (s, 3H, CH_3, encaps.), −1.42 (d, ^3J = 58.5 Hz, 2H, CH_2, encaps.), −1.71 (s, 2H, CH_2, encaps.). TOF MS ES(−) *m*/*z* calcd (found): $Ga_4C_{157}H_{111}N_{13}O_{36}Na_8$ [◆ − $3Na^+$]$^{3-}$, 1071.7742 (1071.7858);

(46) Gottlieb, H. E.; Kotlyar, V.; Nudelman, A. *J. Org. Chem.* **1997**, *62*, 7512–7515.
(47) Alaimo, P. J.; Peters, D. W.; Arnold, J.; Bergman, R. G. *J. Chem. Educ.* **2001**, *78*, 64.
(48) Ellenberger, M. R.; Dixon, D. A.; Farneth, W. E. *J. Am. Chem. Soc.* **1981**, *103*, 5377–5382.
(49) Corey, E. J.; Fuchs, P. L. *Tetrahedron Lett.* **1972**, *13*, 3769–3772.
(50) Capon, R. J.; Barrow, R. A. *J. Org. Chem.* **1998**, *63*, 75–83.

$Ga_4C_{157}H_{108}N_{13}O_{36}Na_7$ [◆ − $4Na^+$]$^{4-}$, 798.0843 (798.0863); $Ga_4C_{157}H_{108}N_{13}O_{36}Na_6$ [◆ − $5Na^+$]$^{5-}$, 633.8695 (633.8650).

K_{11}[8 ⊂ 1]. ^{1}H NMR (500 MHz, D_2O): δ 8.06 (d, ^3J = 7.5 Hz, 12H, Ar−*H*), 7.75 (d, ^3J = 8.5 Hz, 12H, Ar−*H*), 7.70 (d, ^3J = 8.5 Hz, 2H, OTs), 7.36 (d, ^3J = 8.0 Hz, 2H, OTs), 7.33 (d, ^3J = 8.0 Hz, 12H, Ar−*H*), 6.99 (t, ^3J = 8.0 Hz, 12H, Ar−*H*), 6.79 (d, ^3J = 7.0 Hz, 12H, Ar−*H*), 6.62 (t, ^3J = 7.5 Hz, 12H, Ar−*H*), 2.90 (s, 1H, C*H*, encaps.), 1.15 (s, 2H, CH_2, encaps.), 0.62 (s, 3H, CH_3, encaps.), 0.51 (s, 3H, CH_3, encaps.), −0.45 (br, 1H, C*H*, encaps.), −1.0 (s, 3H, CH_3, encaps.), −1.3 to −1.5 (br, 5H, CH_3 + CH_2, encaps.), −1.89 (br, 6H, 2 × CH_3, encaps.). TOF MS ES(−) *m*/*z* calcd (found): $Ga_4C_{157}H_{112}N_{13}O_{36}K_7$ [◆ − $4K^+$]$^{4-}$, 826.288 (826.013); $Ga_4C_{157}H_{113}N_{13}O_{36}K_6$ [◆ − $5K^+$ + H^+]$^{4-}$, 816.799 (816.529); $Ga_4C_{157}H_{114}N_{13}O_{36}K_5$ [◆ − $6K^+$ + $2H^+$]$^{4-}$, 807.310 (807.776).

K_{11}[9 ⊂ 1]. ^{1}H NMR (500 MHz, D_2O): δ 8.06 (d, ^3J = 7.5 Hz, 12H, Ar−*H*), 7.75 (d, ^3J = 8.5 Hz, 12H, Ar−*H*), 7.70 (d, ^3J = 8.5 Hz, 2H, OTs), 7.36 (d, ^3J = 8.0 Hz, 2H, OTs), 7.33 (d, ^3J = 8.0 Hz, 12H, Ar−*H*), 6.99 (t, ^3J = 8.0 Hz, 12H, Ar−*H*), 6.79 (d, ^3J = 7.0 Hz, 12H, Ar−*H*), 6.62 (t, ^3J = 7.5 Hz, 12H, Ar−*H*), −0.3 to −1.1 (many overlapping peaks, encaps.), −1.25 (s, 3H, CH_3, encaps.), −1.55 (s, 2H, CH_2, encaps.), −1.79 (s, 6H, CH_3, encaps.), −1.8 to −2.0 (broad overlapping peaks, encaps.), −2.18 (s, 6H, 2 × CH_3, encaps.). TOF MS ES(−) *m*/*z* calcd (found): $Ga_4C_{157}H_{112}N_{13}O_{36}K_7$ [◆ − $4K^+$]$^{4-}$, 826.288 (826.266); $Ga_4C_{157}H_{113}N_{13}O_{36}K_6$ [◆ − $5K^+$ + H^+]$^{4-}$, 816.799 (816.529); $Ga_4C_{157}H_{114}N_{13}O_{36}K_5$ [◆ − $6K^+$ + $2H^+$]$^{4-}$, 807.310 (807.786).

Kinetic Analyses of Enammonium Rearrangements. Kinetic analyses using equimolar amounts of **1** and the enammonium substrate (Table 1) were performed in D_2O on a Bruker AVB 400 NMR spectrometer. Because of the long reaction times associated with these reactions, kinetic runs were monitored by taking individual time points, and the reaction temperature was maintained outside the probe in an oil bath. The concentration of each sample was 15 mM; the solutions were buffered with 100 mM phosphate buffer and adjusted to pD 8.09. All of the samples were degassed by performing three vacuum/N_2 backfill cycles and sealed under vacuum to prevent the oxidation of **1**. The benzylic methyl peak of the tosylate counterion served as an internal standard for integration. The background reactions of unencapsulated substrates were monitored under the same conditions with regard to substrate concentration, buffer strength, and pD. For the majority of the experiments, the decay of starting material was monitored using 2 scans with a delay time of 25 s and a 90° pulse of 8.15 μs.

When the assembly **1** was exposed to 3 equiv or more of any given propargyl enammonium substrate, significant precipitation occurred. For this reason, DMSO-d_6 (20% by volume) was used as a cosolvent in experiments where substoichiometric amounts of **1** with respect to substrate were used. Kinetic runs using substoichiometric amounts of **1** were performed on Bruker AVB 400, AVQ 400, DRX 500, and AV 500 spectrometers. The concentration of **1** in each sample was 1.7 mM, and the mixed-solvent experiments were conducted without buffer.

Acknowledgment. We thank Dr. Dennis Leung for helpful discussions, Rudi Nunlist for assistance with the NMR experiments, and Drs. Ulla Andersen and Michael Pluth for assistance with mass spectrometry. This research was supported by the Director, Office of Science, Office of Basic Energy Sciences, and the Division of Chemical Sciences, Geosciences, and Biosciences of the U.S. Department of Energy at LBNL under Contract DE-AC02-05CH11231.

Supporting Information Available: Eyring plots for determinations of the activation parameters for the rearrangements of **3** and [**3** ⊂ **1**], saturation data and inhibited saturation data for the catalyzed rearrangement of **3**, and characterization data for the new compounds. This material is available free of charge via the Internet at http://pubs.acs.org.

JA8013055